Butterfly-Inspired Triboelectric Nanogenerators with Spring-Assisted Linkage Structure for Water Wave Energy Harvesting

Rui Lei, Hua Zhai,* Jinhui Nie, Wei Zhong, Yu Bai, Xi Liang, Liang Xu, Tao Jiang, Xiangyu Chen,* and Zhong Lin Wang

The exploration of water wave energy to generate electric power is a promising and valuable way to solve global energy crisis. Triboelectric nanogenerators (TENGs) are considered as one of the most promising approaches for harvesting water wave energy. Here, a butterfly-inspired triboelectric nanogenerator (B-TENG) with spring-assisted four-bar linkage is fabricated to acquire multidirectional water wave energy from different types of movements generated by the device. The arc-shaped outer shell can efficiently absorb the impact force of water wave and inner spring-assisted four-bar linkage can induce multiple contact–separation motion of TENG module, both of which allow the B-TENG to harvest energy from different types of low-frequency waves. The short-circuit current and open-circuit voltage of this B-TENG device can reach 75.35 µA and 707.01 V, while a maximum output power density of 9.559 W m^{-3} can be achieved and 180 light-emitting diodes can be directly lightened up by this B-TENG. The energy generated from this B-TENG can also be stored in a capacitor and to drive some marine sensor devices, such as an electronic thermometer. This proposed B-TENG device is specially designed for multidirectional water energy harvesting and it may have good application prospects for ocean information monitoring and power supply to oceanic islands.

1. Introduction

As the traditional fossil fuel energy resources are increasingly exhausted, the energy crisis becomes a worldwide problem, which results in the urgent demand for the development of renewable techniques.[1] Water wave energy has the promising prospects for producing electrical power on a large scale, since 70% surface of earth is covered by oceans.[2] However, the traditional electromagnetic generators for harvesting water wave energy have some limitations, such as bulky structure, high fabrication cost, and insufficient energy conversion capability at low frequency.[3] Therefore, searching a new type of conversion method for harvesting water wave energy can be a real challenge.[1a,4] The emergence of triboelectric nanogenerator (TENG) provides a new possibility for effectively harvesting water wave energy due to its high conversion efficiency at low frequency state (especially 0.1–3 Hz).[2,5] Meanwhile, low fabrication cost and design flexibility of TENG can further facilitate its development in the industrialization direction.[6] Originated from the Maxwell's displacement current,[7] TENG can convert mechanical energy from environment to electricity[8] by utilizing the coupling effect of triboelectrification and electrostatic induction.[9] So far, a variety of TENGs have been designed to harness low frequency energy in the water wave[10] and the maximum power density of the device has been updated almost every two months.

R. Lei, Prof. H. Zhai
Anhui Province Key Lab of Aerospace Structural Parts Forming Technology and Equipment
Hefei University of Technology
Hefei, Anhui 230009, P. R. China
E-mail: jxzhaihuajx@sina.com

R. Lei, Prof. H. Zhai
Institute of Industry & Equipment Technology
Hefei University of Technology
Hefei, Anhui 230009, P. R. China

J. Nie, W. Zhong, Y. Bai, X. Liang, Dr. L. Xu, Dr. T. Jiang, Prof. X. Chen, Prof. Z. L. Wang
Beijing Key Laboratory of Micro-Nano Energy and Sensor
Beijing Institute of Nanoenergy and Nanosystems
Chinese Academy of Sciences
Beijing 100083, P. R. China
E-mail: chenxiangyu@binn.cas.cn

J. Nie, W. Zhong, Y. Bai, X. Liang, Dr. L. Xu, Dr. T. Jiang, Prof. X. Chen, Prof. Z. L. Wang
School of Nanoscience and Technology
University of Chinese Academy of Sciences
Beijing 100049, P. R. China

Prof. Z. L. Wang
School of Material Science and Engineering
Georgia Institute of Technology
Atlanta, GA 30332-0245, USA

**ADVANCED
SCIENCE NEWS**

www.advancedsciencenews.com

**ADVANCED
MATERIALS
TECHNOLOGIES**

www.advmattechnol.de

The sphere–spring-assisted multilayer structure[11] and the spring-assisted structure[12] have been previously introduced to the design of TENG, which greatly enhanced the output performance of TENGs for harvesting water wave energy. The spring-assisted structure can induce multiple motion cycles in the TENG device and thus, TENGs can have enough opportunities to recycle the motion energy. The optimized motion transformation component with the spring-like structure can convert the wave motion into the all kinds of desired motion behaviors in TENG and the mechanical energy can be fully recycled by the electrostatic field inside TENG. Nevertheless, as for spring-assisted structure, power can only be generated when the device is driven in swinging with fixed direction of water wave propagation. Meanwhile, for sphere–spring-assisted multilayer structure, even though the direction of water wave propagation can be satisfied, the motion behavior of the device should be better in fluctuating condition rather than in swing condition. With the consideration of all these factors, more efforts should be focused on the structure modification of the motion conversion part of TENG.

In this study, we designed a novel butterfly-inspired TENG (B-TENG) device for acquiring multidirectional ocean wave energy from different types of movements generated by the device. In this device, a spring-assisted four-bar linkage with four double-faced copper-clad plastic sheets wings is placed in a double arc–shaped case body, which allows the device to trigger the motion with two different patterns. These motions can cause the TENG to work in the contact–separation mode and the mechanical energy of water wave can be converted into electricity based on the induction effect between the copper electrode and polytetrafluoroethylene (PTFE) films. Experiments had been performed in the real water wave to investigate the influences of several key factors to the TENG performance, such as wave frequency and water wave propagation direction. Given the great performance of multidirectional wave energy harvesting, the device can achieve a high electrical output with open-circuit voltage (V_{oc}) of 707.01 V, short-circuit current (I_{sc}) of 75.35 µA, and power density of 9.559 W m^{-3}, which can further promote the application study of TENG for harvesting blue energy.

2. Results and Discussion

2.1. Construction of B-TENG

A schematic structure of the B-TENG device for water wave energy harvesting is shown in **Figure 1**a. The B-TENG device
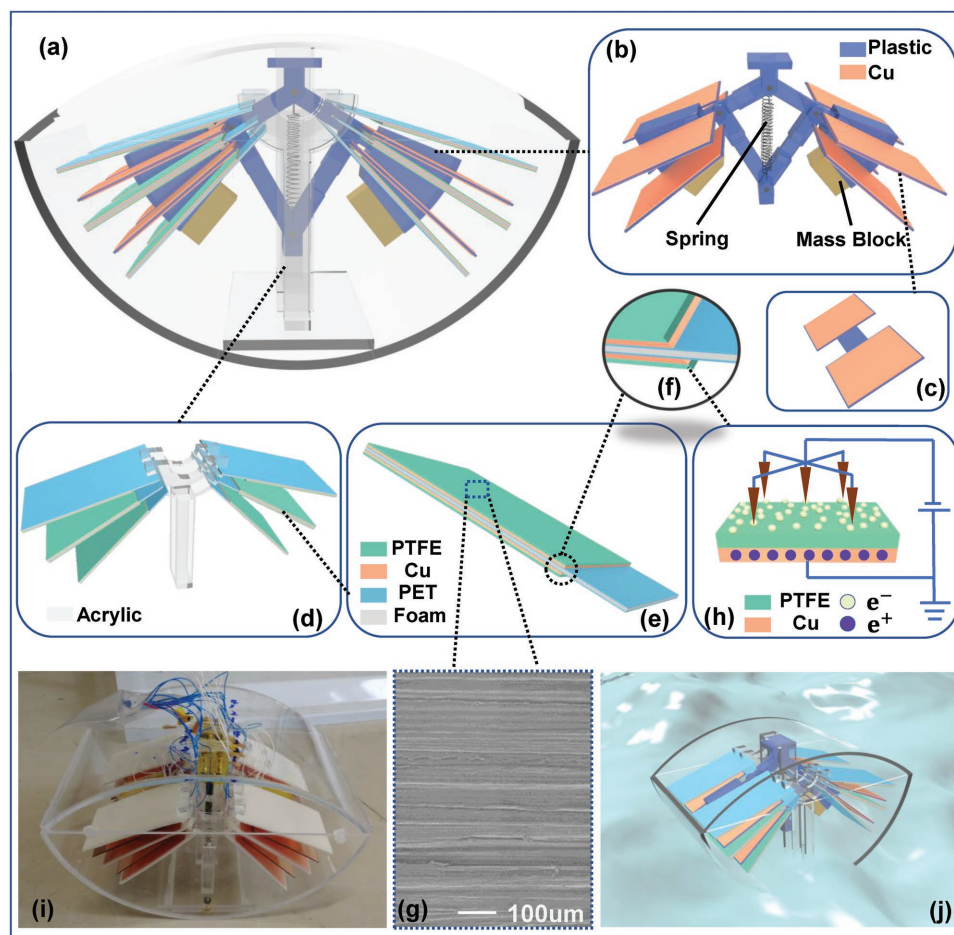

Figure 1. a,j) Schematic diagram of the B-TENG device. b,c) Schematic diagram of the four-bar linkage with wings and mass blocks. d–f) Detail structure of Y-bracket module and SBM. g) SEM image of the PTFE film surface after stretching treatment. h) Schematic the electron injection process for generating negative charges on the surface of PTFE. i) Photograph of the fabricated B-TENG device.

is mainly composed of two components: the inner TENG module and the outer shell. In the inner TENG module, we designed two parts to induce contact and separation motions, which are spring-assisted four-bar linkage with mounted wings (SFLW) and the Y-shaped bracket with the inlaid soft base module (Y-bracket module). The detailed fabrication process of the B-TENG device can be found in the Experimental Section and the installation progress of device is illustrated in Figure S1 (Supporting Information), respectively. In Figure 1b, the four-bar linkage of SFLW is a symmetrical rhombic four-bar mechanism with four links and each two adjacent links connected by hinged shaft, which makes the whole mechanism easy to be deformed. As can be seen in Figure 1b, we can define the shaft connecting the two long links as shaft-1 and the shaft linking the two short links is shaft-2. The shaft-1 and the shaft-2 of the four-bar mechanism are connected by a spring, and then the spring-assisted four-bar linkage (SFL) is formed. When triggered by external forces, the SFL structure can be easily restored to its original state due to the restoring force of spring. In order to enhance the deformation of the device, two mass blocks are added to the end of two long links, which can amplify the deformation of the SFL under external forces. Figure 1c shows the structure of a single wing, which is cut into H shape. By setting two slots at each end of two long links in the SFL, 4 H-type wings can be embedded into the SFL to form SFLW, and the embedded structure reduces the overall size of SFLW. As shown in Figure 1c, the H-type single wing is divided into two small sheets. Each small sheet is covered with double-sided copper clad, so that the SFLW contains 16 copper foils. A fixed block is connected to the acrylic gantry, and the shaft-1 is mounted in the fixed block so that the SFLW can be hung on the gantry. The SFLW can generate two working states under external excitation: the reciprocating swing around shaft-1 and the flapping motion with shaft-1 as the fixed axis.

In Figure 1d, the Y-bracket module is a Y-shaped symmetrical sample holder embedded with 6 soft base modules (SBMs). Figure 1e shows the detail structure of SBM, that the base is attached with double-sided PTFE–Cu film. From the enlarged view of the base in Figure 1f, a foam layer is sandwiched between two polyethylene terephthalate (PET) slices to improve the contact intimacy between tribomaterials. As shown in Figure 1d, 6 SBMs with 8 PTFE–Cu films are embedded in 1 Y-bracket. PTFE film is the dielectric material for triboelectrification in our experiment and it has a raw thickness of 50 μm. In order to induce the rough surface for increasing the effective contact area, stretching treatment is applied for the raw PTFE film. The film is stretched in one direction for 200%, while the width of the film is kept unchanged during the stretching treatment. Accordingly, the final thickness of the PTFE film becomes ≈25 μm and the induced stripe structure on the surface can facilitate the electrification process. The scanning electron microscope (SEM) image of the PTFE film surface after stretching treatment is shown in Figure 1g. A polarization method is also employed to inject electrons into the top surface of PTFE film and the experimental setup for electron injection on the PTFE surface process[12a,13] is schematically shown in Figure 1h. The needle array is connected to the cathode of the high voltage source, while the Cu electrode beneath the PTFE film is connected to the ground. With the applied high voltage (6 kV), numerous electrons are injected from the needle point to the PTFE film surface, which can enhance the surface charge density during the tribomotion. In the real operation, the Y-bracket as well as SBM with PTFE films is fixed with the shell and the SFLW is the active component that integrated with the Y-bracket module. The swing and flapping motion of the SFLW leads to the contact–separation motion between the Cu foils on the SFLW and the PTFE films on the Y-bracket module. Accordingly, the electrode located on both the SFLW and the Y-bracket module can generate electrical signal based on the electrostatic induction effect. For the structure design, the number of the wings can be adjusted, and the number can be increased on the basis of the original. The size of the wings is decided by the volume of the outer shell. The weight of the mass is the optimized value based on the current design. The inclined angle of sealed B-TENG surface drawing on the design of the nod duck structure has been demonstrated by previous study.[14] Since the current research is the first report about B-TENG, a series of continuous work will be done to further modify the device for better performance and a more suitable size. The TENG module is sealed by the transparent shell to form the complete device, as shown in Figure 1a. Inspired by the previous studies,[14] the shell of whole device is designed as a double arc–shaped body, and the acrylic shell would be inclined or fluctuated cyclically in the water wave due to the shape of the shell. Figure 1i is the real photograph of the device. After encapsulation and waterproof treatment, the device can be put into water to collect wave energy, as can be seen in Figure 1j. Based on the structure of the outer shell, the water wave can trigger two kinds of motion for B-TENG, the undulating fluctuation and the swing motion. The fluctuating state of device is similar to the state of sphere–spring-assisted multilayer structure,[11] while the swing state of device is similar to energy harvesting of the duck-shaped triboelectric nanogenerator.[14a] The B-TENG device with multiple working states can carry forward the advantages of other TENG devices, providing more possibilities for efficient wave energy harvesting.

The multiple motion states of B-TENG device in the water wave can also induce different motion states of the TENG module. In order to further elaborate the motion states of the TENG module inside the device, we analyze the dynamic behavior of the SFLW under the excitation of external forces. The SFLW can produce two motion states: up and down reciprocating flap and back and forth reciprocating oscillation. These two kinds of motion states of the SFLW promote the movement of the wings, so that the Cu foils on the surface of the wings is in contact–separation with the PTFE–Cu films. **Figure 2**a shows eight sets of TENG units in front view. For the flapping mode, the wings of TENG module are moving up and down and the mechanism of energy generation in four individual contact-pair units is illustrated in Figure 2b. At State-I, the Cu electrode on the surface of wings is in full contact with the PTFE film. Due to the triboelectrification effect, positive charges are accumulated on the Cu surface, while negative charges transfer to the PTFE surface. When the spring restoring force causes the mass blocks to move up, the Cu foil as well as the wing is separated from the PTFE film and the potential difference between the two surfaces is
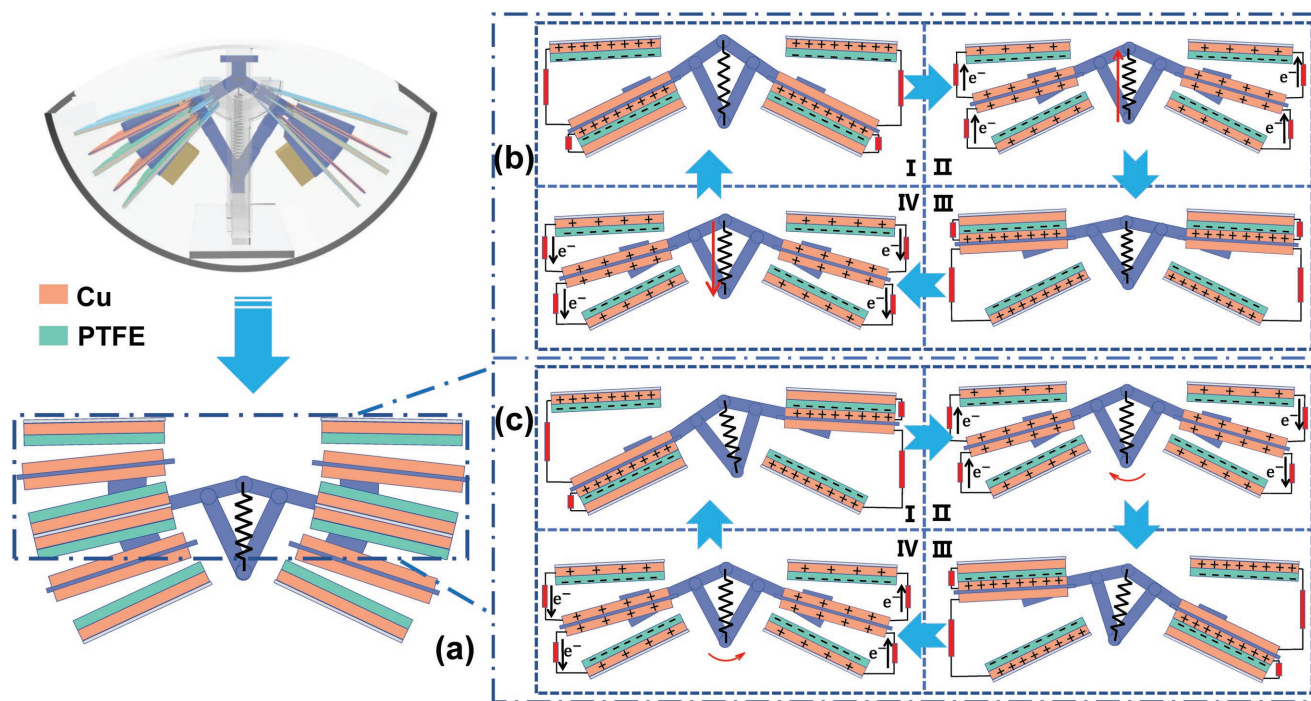
Figure 2. a) Schematic diagram of the spring-assisted four-bar linkage with wings. b,c) Working principle of the simplified spring-assisted four-bar linkage with wings in flap mode and swing mode, respectively.

established, which can drive electrons from the electrode on the back side of the PTFE film to the Cu foil and generate an instantaneous current (State-II). As the mass blocks continues to move up, the separation distance between the Cu foil and the PTFE surface continues to increase. When the distance between the Cu foil and the PTFE surface reaches the maximum value, the charge transfer reaches saturation (State-III). When the mass blocks reach the highest point, the mass blocks begin to fall down under gravity and spring tension. Accordingly, the distance between the Cu foil and the PTFE surface starts to decrease and the established electrical potential starts to decrease. When the Cu foil is in contact with the PTFE film again, the charge is neutralized. Similarly, the power generation principle of the TENG module in back and forth reciprocating oscillation is shown in Figure 2c, where the only difference is the motion mode of the wings. For the real operation, all 16 units on TENG module are connected in parallel to achieve the final output, where all the Cu foils on the moving wings are connected as the positive output end and all the Cu electrodes under PTFE films are connected together as the negative output end. The TENG unit of the entire device employs a nonparallel contact–separation mode, and each TENG structure employs a conductive–dielectric material category. Furthermore, to obtain a more quantitative understanding of the electricity generating process, two theoretical models with the same dimensions as the real device was established by using COMSOL Multiphysics. The electric potential distribution of every component during the continuous movement of B-TENG by a finite element simulation is observed, and the established potential drop reaches 10 000 V, as shown in Figure S2 (Supporting Information).

2.2. Acquiring Energy from Different Types of Movement on Linear Motor

It is important to note that the B-TENG should be tested in the real water wave for calibrating its output capability. Meanwhile, in order to clearly study the motion behavior of TENG module, we first test the device under the drive of linear motor to simulate the effective external forces, where the detailed motion parameters can be precisely controlled by software. The B-TENG device subjected to three directional movements had been performed by external forces: horizontal back and forth movement of the device; overall swing along the curved surface of shell; and vibration up and down of device. As mentioned in Figure 2, all these external forces applied on the outer shell can cause the TENG module to produce two kinds of movements: wing flapping and swing oscillation. The horizontal movement and the swing mode of the outer shell leads to the swing motion of TENG module around the shaft-1, while the up and down vibration of the outer shell drives the TENG module to flap up and down. The relevant test results are placed in **Figure 3** and Figure S3 (Supporting Information), and the test method can be viewed in Video S1 (Supporting Information).

The maximum displacement of the linear motor is fixed to be 6 cm with the maximum speed of the device to 5 m s^{-1}, and the effect of different acceleration on the electrical performance of the B-TENG is studied. As shown in Figure 3a-I, the acceleration of the device is increased from 2.5 to 7.5 m s^{-2}, and the maximum peak value of the transferred charge Q_{sc} of the device is gradually increased from 0.71 to 1.347 µC. It should be noted that the acceleration starts from 2.5 m s^{-2} due to the large stiffness of spring. For small accelerations, such

**ADVANCED
SCIENCE NEWS**
www.advancedsciencenews.com

**ADVANCED
MATERIALS
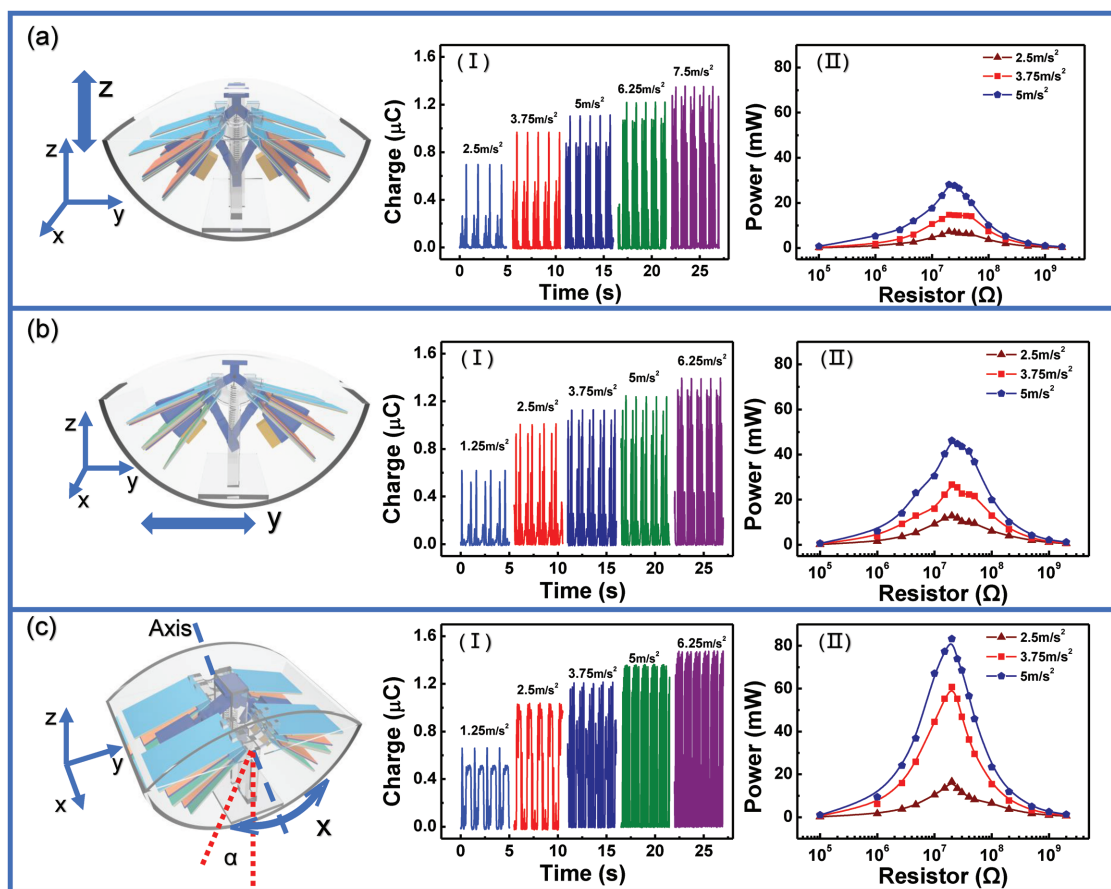TECHNOLOGIES**
www.advmattechnol.de

Figure 3. a–c) Schematic diagram of the B-TENG device in vibration up and down, horizontal back and forth movement, swing mode, respectively. a-I–c-I) Transferred charge of the B-TENG device driven by linear motor in vibration up and down, horizontal back and forth movement, swing mode, respectively. a-II–c-II) Output power of the B-TENG device driven by linear motor in vibration up and down, horizontal back and forth movement, swing mode, respectively.

as at 1.25 m s^{-2}, the mass blocks do not have enough kinetic energy to make the wings to fully contact with the base, which results in the insufficient power generation cycle. The I_{sc} is determined by the motion speed and the amount of Q_{sc}. As can be seen from Figure S3(a–c) (Supporting Information), when the acceleration is increased from 2.5 to 7.5 m s^{-2}, the maximum peak value of the I_{sc} is gradually increased from 48.1 to 144.6 µA, and the V_{oc} is increased from 701.5 to 1334.1 V. The increase of the I_{sc} and V_{oc} with the increase of acceleration can be explained by the structure design of spring-assisted SFLW, where the higher acceleration can induce stronger impact force on the contact surface and thus enhance the triboelectrification process. In order to test the output power of the device, we use different resistors as the load in the circuit. The relationship between the average peak power and the external resistor is shown in Figure 3a-III. The output power increases with the increase of acceleration and the maximum peak power of the device is 28.125 mW at the matched resistance of 20 MΩ with an acceleration of 5 m s^{-2}. Subsequently, the output characteristics and power output of the device periodically moves in horizontal direction are also explored. The specific experimental method can also refer to Video S1 (Supporting Information). In the horizontal back and forth movement mode,

the maximum horizontal displacement of the device was 6 cm and the acceleration range from 1.25 to 6.25 m s^{-2}. As can be seen from Figure 3b-I, many small peaks in each cycle are captured. This is due to the bouncing motion of wings induced by the elastic base. When the device moves horizontally back and forth, the wings can contact with the base multiple times. In the horizontal movement mode, we also measure average output power with different external resistance, which can be seen in Figure 3b-II for details. In the swing mode, the incline angle of the device is fixed to be 32°. For linear motor settings, the acceleration is gradually added from 1.25 to 6.25 m s^{-2}. As the acceleration increases, the transferred charges increased in the same ways as the previous two cases (see Figure 3c-I). The relationship between the average peak power in the swing mode and the external resistor is shown in Figure 3c-III, where the acceleration is 5 m s^{-2}, the average peak power of the device reaches 83.205 mW, with the matching resistance 20 MΩ.

Based on the results in Figure 3a–c, we can find that the device in swing mode can generate the highest output, while the lowest output is obtained from flapping mode. This is because when the device is in the flapping mode, the stretching and compressing motion of spring consume part of the kinetic energy, causing the decrease of output. Meanwhile, for the
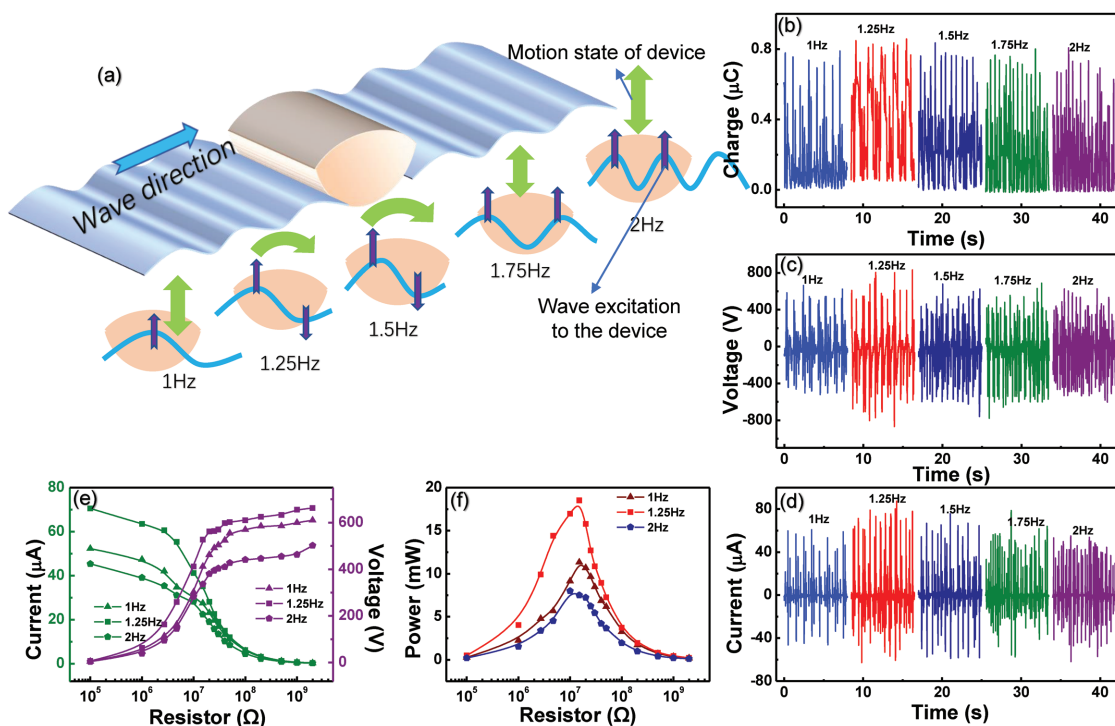
**ADVANCED
SCIENCE NEWS**
www.advancedsciencenews.com

**ADVANCED
MATERIALS
TECHNOLOGIES**
www.advmattechnol.de

Figure 4. a) Schematic diagram of the B-TENG when the flat surface of the device is in parallel with the incident water wave b–d) output voltage, transferred charges, and output current of the B-TENG device under the water waves. e,f) Dependence of the output power of the TENG unit on resistive loads for different frequencies.

horizontal movement of the device, although the internal power generation module operates in the same principle, the output of the device in horizontal movement is lower than that in the swing mode. This is due to the less gravitational energy conversion of mass blocks during swing motion. The influences of displacement and incline angle to the output performance are also considered. The transferred charges for the B-TENG as a function of the vertical displacement are shown in Figure S3a-I (Supporting Information). When the vertical displacement increases from 15 to 90 mm, the peak value of transferred charge increases first and then saturates. Similar phenomenon can also be seen in Figure S3b-I (Supporting Information) when changing the horizontal displacement. Moreover, the output transferred charges are growing slowly with the increasing angle of inclination for device, which is shown in Figure S3c-I (Supporting Information). This phenomenon is due to the more sufficient contact–separation of TENG units with the increase in displacement and angle.

2.3. B-TENG Operating in Real Water Wave

After sealing and waterproof treatment, the B-TENG is placed in a water tank to test the performance for real water wave energy collection. Pervious work shows that when the TENG-related device is tested in a water wave environment, the humidity can affect the output performance of the device,[15] and the output performance of the device gradually decreases with the humidity increases. Therefore, in this work, we put some anhydrous silica inside the device to keep the internal

environment dry during the sealing process. In the water tank, the water pumps are controlled by digital signal to create water waves with the desired parameters. The frequency and amplitude of the water wave are controlled by the output frequency and output amplitude of the signal source. As shown in **Figure 4**a, the flat surface of the device is in parallel with the incident water wave and the influences of different water wave frequencies on the output performance of the B-TENG are explored. The water wave frequency is ranged from 1 to 2 Hz, and the output performances of the device are measured every 0.25 Hz. When the frequency of applied water wave is 1, 1.75, and 2 Hz, the device shows oscillating motion in up and down direction. When the frequency of applied water wave is 1.25 and 1.5 Hz, the device shows swing motion. The specific motion status can be referred to Video S2 (Supporting Information). The Q_{sc}, I_{sc}, and V_{oc} of the device under different frequency water waves are shown in Figure 4b–d, and the uncertainty of the data is mainly caused by the random fluctuation of water wave (so 8 s were taken in each frequency to show the stability of output performance of device). We can see that the output signal can reach average maximum value at 1.25 Hz, where Q_{sc} reaches 0.838 μC, I_{sc} reaches 75.35 μA, and V_{oc} reaches 707.01 V. As can be seen in Video S2 (Supporting Information), the incline angle of the device is close to 50° at the frequency of 1.25 Hz and the incline angle of device is only 30° at the frequency of 1.5 Hz. After detecting the output performance of the device, different resistors can be connected as loads into the circuit. Figure 4e reflects the relationship between the average peak current and the average peak voltage of the device when different loads are connected to the device, and Figure 4f
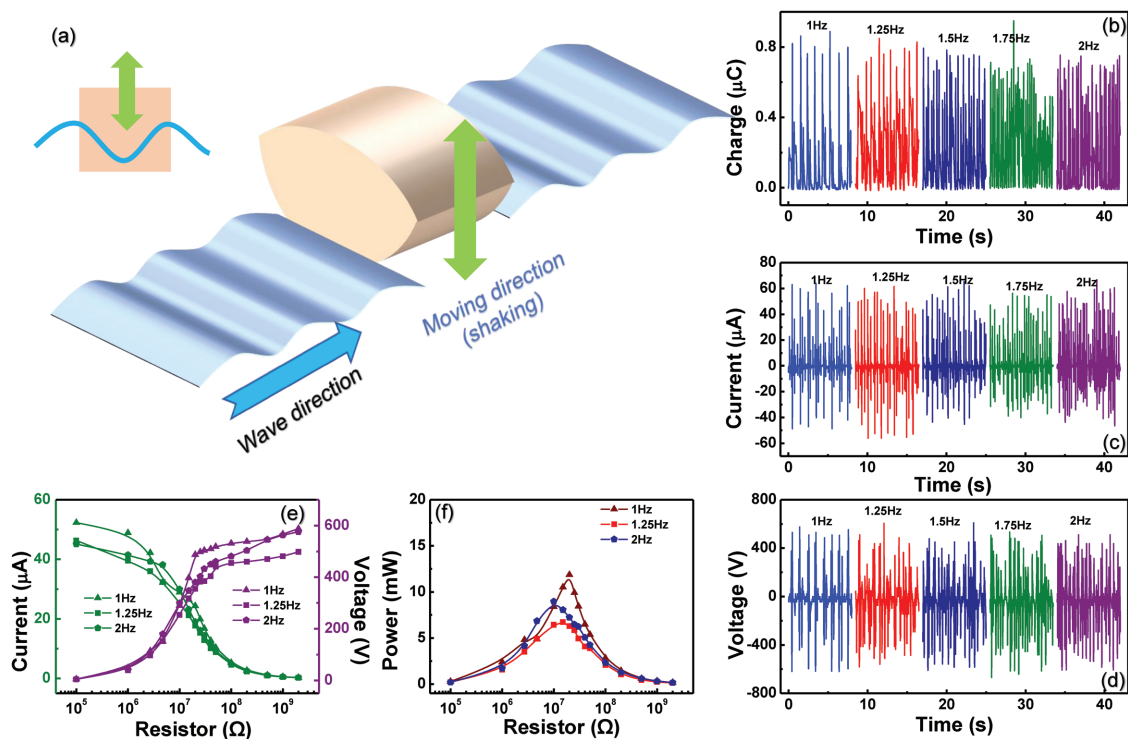
Figure 5. a) Schematic diagram of the B-TENG device in wave condition when the flat surface of the device is in perpendicular with the incident water wave b–d) transferred charges, output current, and output voltage of the B-TENG device under the water waves. e,f) Dependence of the output power of the TENG unit on resistive loads for different frequencies.

illustrates the relationship between the average output power of the device and the resistance at different water wave frequencies. Figure 4e,f does not fully display the corresponding output values of device for all water wave frequencies, so the supplements are shown in Figure S4a,b (Supporting Information). Combined with Figure 4f and Figure S4a (Supporting Information), the device shows the highest performance that the average output power is 18.509 mW when the water frequency is 1.25 Hz, and the matching resistance is 15 MΩ. With the consideration of the volume of the device, average power density at this time reaches 9.559 W m^{-3}. Considering the effective area of the TENG, the areal power density of the device is 0.712 W m^{-2}.

When the flat surface of the device is perpendicular to the direction of the water wave, the motion behavior of the B-TENG device is quite different from the above case. Therefore, we further study the motion state and output of the device, when it is in the vertical direction of the water wave, as shown in **Figure 5**a. For the water wave in this direction, only oscillation motion of the device can be triggered. Figure 5b–d shows the output of the Q_{sc}, I_{sc}, and V_{oc} at different water wave frequencies, and output of the device is relatively stable within a certain range of water frequency frequencies under oscillation motion. In this wave incident direction, the device exhibits the maximum outputs at the water wave frequency around 1 Hz. The Q_{sc} can reach 0.768 μC, the highest I_{sc} is 58.297 μA, and the related V_{oc} can be 617.1 V. Meanwhile, the output of device becomes the minimum at 1.75 Hz. Figure 5e reflects the changing of the peak current and the peak voltage

of the device in response to different external load and different wave frequencies. Moreover, Figure 5f shows the relationship between the average output power and different wave frequencies. At 1 Hz, the highest output power of the device reaches 11.87 mW and the matching resistance is 20 MΩ. It also should be noted that Figure S4c,d (Supporting Information) is the supplement of Figure 5e,f which does not fully display the corresponding output values of device for all water wave frequencies.

Finally, a rectifying circuit is applied to B-TENG for establishing an effective charging system, as can be seen in **Figure 6**a. 4 rectifier bridge modules are connected to the output ends of TENG. The rectified current with only one polarity can be obtained, when the flat surface of the device is in parallel with the incident water wave, as shown in Figure 6b. After the device is rectified, 180 light-emitting diodes (LEDs) can be lightened up by using this device to collect water wave energy, as shown in Figure 6c and Video S3 (Supporting Information). In order to demonstrate the energy generation capability of this B-TENG, we use the output signal from this B-TENG to charge the commercial capacitors (see Figure 6d). The charging and discharging performances of the TENG–capacitor system are shown in Figure 6e,f. With the excitation from water wave, the B-TENG device can charge capacitors with different capacitances. The charging rate curve is shown in Figure 6e, where the frequency of water wave is fixed to be 1.75 Hz. Here, a capacitor with a capacity of 470 μF has been chosen as the storage component to power the digital thermometers. After the charging process supported by B-TENG, the capacitor is able to successfully power the thermometer to display the
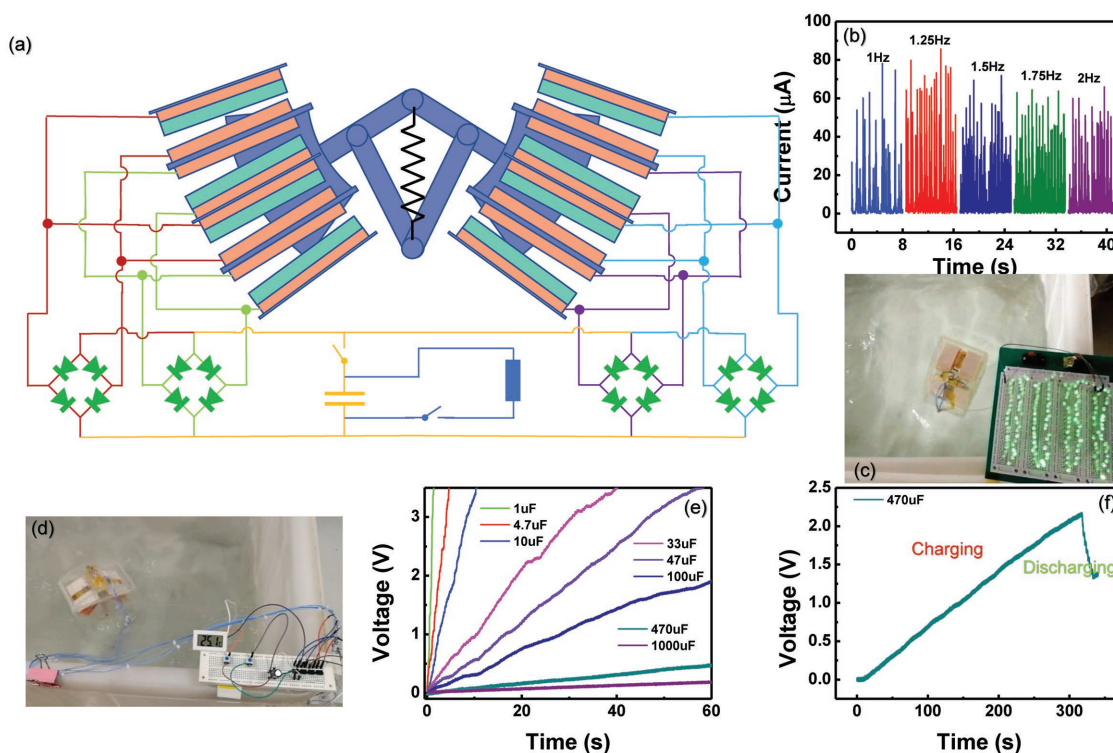
**ADVANCED
SCIENCE NEWS**

www.advancedsciencenews.com

**ADVANCED
MATERIALS
TECHNOLOGIES**

www.advmattechnol.de

Figure 6. a) Schematic diagram of the circuit connected electrically in parallel through four rectifier bridges. b) Rectified output current of the B-TENG device at various frequencies of water waves when arched surface of device was set to face wave direction. c) Photograph of dozens of LEDs which are lighted up by the B-TENG device under the water wave motions. d) Photograph of an electronic thermometer driven by the B-TENG device under the water wave motions through charging a capacitor of 470 μF. e) The voltage of various capacitors charging by the B-TENG. f) The charging and discharging processes of a capacitor of 470 μF by the B-TENG under the water waves.

right temperature of the water, which is shown in Video S4 (Supporting Information) and Figure 6f. The charging time for a capacitor of 470 μF from 0 to 2.3 V is about 310 s by using the B-TENG. Then, the capacitor discharging by lighting the digital thermometer and the capacitor voltage is immediately dropped down to about 1.5 V as the thermometer is initialized for the operation. These results show that this TENG device can be used as a floating energy package, and it may have good application prospects for marine sensor devices. Meanwhile, a series of this kind of B-TENG can be integrated together as the generator arrays and a lot of tiny energy can be gathered to achieve a notable and useful energy generation. We also believe that the proposed communication system has great potential to meet the requirements of the real application by using more advanced micro- or nanofabrication technology. On the other hand, it is important to note that the device reported in this paper is just a prototype for demonstrating the mechanism of power generation. The experiments in the real water wave are much more difficult than that in the lab. First of all, we need to consider the detailed condition of the water, such as water quality and underwater environment. In that case, the outer shell made by acrylic plastics cannot withstand long-time operation. However, if we apply some corrosion-resistant materials for fabricating the shell, we need to carefully balance the weight and the cost in order to maintain the advantages of TENG technique. Moreover, if we want to transport a harvested energy to a remote place in the water, the electrical lines for power transfer

can also cause trouble. All these challenges must be solved before this technique can really get into the real application and we will focus on these topics in our future studies.

3. Conclusion

In summary, we designed a B-TENG device using spring-assisted four-bar linkage for multidirectional water wave energy harvesting from different types of movements generated by device. The spring-assisted four-bar linkage can utilize the motion of the outer shell and induce two kinds of movements for TENG module: wing flapping and swing oscillation. Both the movements can generate electrical energy based on the contact and separation motion between the Cu electrode and PTFE film in the TENG module. The influences of the water wave frequency to the output performance of B-TENG device are investigated. In water wave, the highest outputs of this TENG units are obtained at 1.25 Hz, when the flat surface of the device is in parallel with the incident wave. The maximum output power density can reach 9.559 W m^{-3} with the matched resistance of 15 MΩ. For the demonstration, dozens of LEDs (about 180 lights) are lighted up by the floating B-TENG in the wave. Meanwhile, the electrical energy from this B-TENG is enough to charge some capacitors and the charged capacitor can be used to power an electronic thermometer, indicating the potential application of this TENG for the sensor devices

in the ocean. This work could provide useful information for the multidirectional harvesting water wave energy, making the water wave energy harvesting more efficient.

4. Experimental Section

Fabrication of the TENG Units: The single contact-pair TENG unit for this experiment had two objects (a fixed one and a moveable one) to serve as motion parts. As the moveable one, the 1 mm thickness plastic sheet as wing was cut into H section by laser cutters to form four 50 mm × 65 mm surfaces, and each top surface was attached on a dimension of 50 mm × 65 mm copper foil as the tribosurface and the output electrode. A flexible foam layer with a dimension of 50 mm × 80 mm × 1 mm was sandwiched between two 50 mm × 80 mm × 0.2 mm PET slices act as the substrate of TENG unit and to be fixed, and the PTFE–Cu film was adhered on the top surface of substrate. There were two kinds of PTFE–Cu film covered substrate, one was the PTFE–Cu film only adhered on the single side of substrate (S-F NE), the other was double side of the substrate were both covered with PTFE–Cu film (D-F NE). It was noted that the initial thickness of PTFE film was ≈50 µm, while the final thickness was nearly 25 µm after stretching PTFE film in one direction for 200%. Then, a needle array constituted of 5 parallel connected needles was placed above the surface of PTFE–Cu film with a height of 10 mm, and the needle array was connected to the cathode, the Cu foil under PTFE was linked to the anode and ground. By applying a polarization voltage of 6 kV for 8 min, electrons were injected to the top surface of PTFE film.

Fabrication of the TENG Device: The main structure of moving parts in B-TENG device was a four-bar linkage (FBL) made of plastic, where a rigid spring linked the top and bottom axis of the FBL. At the end of the longest two linkages, two slots were designed for each linkage to insert the wings and the angle between two adjacent wings is 16°. To balance the tension of spring and enhance the deformation of the FBL, two 160 g mass blocks were adhered on the bottom of the longest linkage each side. Then, the whole spring-assisted FBL was hanging on an acrylic gantry. The designed Y-type acrylic stereo bracket(Y-bracket) had 6 slots are distributed symmetrically on its left and right side to insert PTFE–Cu film–covered substrate. Taken one side of Y-bracket as an example, two S-F NEs were embedded in upper slot and bottom slot, respectively, while the D-F NE was inserted in middle slot. Note that the PTFE–Cu films adhered on two S-F NEs are placed face to face, and the angle between the two adjacent substrates was 16°. Two Y-brackets embedded with PTFE–Cu film–attached substrates were parallelly distributed on both side of the spring-assisted FBL, and each wing was successfully placed in the middle of two adjacent substrates at the initial state with 16 TENG units constructed. Y-brackets and acrylic gantry were stuck on a 120 mm × 55 mm × 4 mm acrylic base, and the whole structure was set in a double arc–shaped case body. The case body was composed with a 4 mm thickness semiarc acrylic shell with the diameter of ⌀ 190 mm and another 4 mm thickness semiarc acrylic shell with the diameter of ⌀ 295 mm, and the composite shell was in 190 mm × 120 mm × 120 mm size. Finally, after adding anhydrous silica gel, the shell was sealed and waterproofed and processed for water wave energy harvesting.

Electrical Measurement of the TENG Output Performance: The output voltage signals of the device were measured by a digital oscilloscope (Agilent InfiniiVision DSO-X 2014A), and the output current, transferred charges were measured by a current preamplifier (Keithley 6514 System Electrometer).

Supporting Information

Supporting Information is available from the Wiley Online Library or from the author.

Conflict of Interest

The authors declare no conflict of interest.

[1] a) J. P. Painuly, *Renewable Energy* **2001**, *24*, 73; b) M. Z. Jacobson, M. A. Delucchi, G. Bazouin, Z. A. F. Bauer, C. C. Heavey, E. Fisher, S. B. Morris, D. J. Y. Piekutowski, T. A. Vencill, T. W. Yeskoo, *Energy Environ. Sci.* **2015**, *8*, 2093; c) X. Chen, L. Liu, Y. Feng, L. Wang, Z. Bian, H. Li, Z. L. Wang, *Mater. Today* **2017**, *20*, 501.

[2] Z. L. Wang, *Nature* **2017**, *542*, 159.

[3] a) A. Wolfbrandt, *IEEE Trans. Magn.* **2006**, *42*, 1812; b) R. Henderson, *Renewable Energy* **2006**, *31*, 271.

[4] O. Ellabban, H. Abu-Rub, F. Blaabjerg, *Renewable Sustainable Energy Rev.* **2014**, *39*, 748.

[5] a) Z. L. Wang, T. Jiang, L. Xu, *Nano Energy* **2017**, *39*, 9; b) Z. L. Wang, J. Chen, L. Lin, *Energy Environ. Sci.* **2015**, *8*, 2250.

[6] a) G. Zhu, Y. S. Zhou, P. Bai, X. S. Meng, Q. Jing, J. Chen, Z. L. Wang, *Adv. Mater.* **2014**, *26*, 3788; b) F.-R. Fan, Z.-Q. Tian, Z. L. Wang, *Nano Energy* **2012**, *1*, 328.

[7] Z. L. Wang, *Mater. Today* **2017**, *20*, 74.

[8] a) Y. Feng, L. Ling, J. Nie, K. Han, X. Chen, Z. Bian, H. Li, Z. L. Wang, *ACS Nano* **2017**, *11*, 12411; b) D. H. Kim, H. J. Shin, H. Lee, C. K. Jeong, H. Park, G.-T. Hwang, H.-Y. Lee, D. J. Joe, J. H. Han, S. H. Lee, J. Kim, B. Joung, K. J. Lee, *Adv. Funct. Mater.* **2017**, *27*, 1700341; c) Y. Xi, H. Guo, Y. Zi, X. Li, J. Wang, J. Deng, S. Li, C. Hu, X. Cao, Z. L. Wang, *Adv. Energy Mater.* **2017**, *7*, 1602397; d) Z. Ren, J. Nie, J. Shao, Q. Lai, L. Wang, J. Chen, X. Chen, Z. L. Wang, *Adv. Funct. Mater.* **2018**, *28*, 1802989; e) L. Xu, H. Wu, G. Yao, L. Chen, X. Yang, B. Chen, X. Huang, W. Zhong, X. Chen, Z. Yin, Z. L. Wang, *ACS Nano* **2018**, *12*, 10262.

[9] a) X. Chen, Y. Wu, A. Yu, L. Xu, L. Zheng, Y. Liu, H. Li, Z. L. Wang, *Nano Energy* **2017**, *38*, 91; b) L. Zheng, Y. Wu, X. Chen, A. Yu, L. Xu, Y. Liu, H. Li, Z. L. Wang, *Adv. Funct. Mater.* **2017**, *27*, 1606408; c) J. Nie, Z. Ren, Y. Bai, J. Shao, T. Jiang, L. Xu, X. Chen, Z. L. Wang, *Adv. Mater. Technol.* **2018**, *3*, 1800300; d) J. Nie, Z. Ren, J. Shao, C. Deng, L. Xu, X. Chen, M. Li, Z. L. Wang, *ACS Nano* **2018**, *12*, 1491.

[10] a) J. Chen, J. Yang, Z. Li, X. Fan, Y. Zi, Q. Jing, H. Guo, Z. Wen, K. C. Pradel, S. Niu, Z. L. Wang, *ACS Nano* **2015**, *9*, 3324; b) X. F. Wang, S. M. Niu, Y. J. Yin, F. Yi, Z. You, Z. L. Wang, *Adv. Energy Mater.* **2015**, *5*, 1501467; c) Y. Yao, T. Jiang, L. Zhang, X. Chen, Z. Gao, Z. L. Wang, *ACS Appl. Mater. Interfaces* **2016**, *8*, 21398; d) L. Xu, Y. Pang, C. Zhang, T. Jiang, X. Chen, J. Luo, W. Tang,

**ADVANCED
SCIENCE NEWS**

www.advancedsciencenews.com

**ADVANCED
MATERIALS
TECHNOLOGIES**

www.advmattechnol.de

X. Cao, Z. L. Wang, *Nano Energy* **2017**, *31*, 351; e) B. D. Chen, W. Tang, C. He, C. R. Deng, L. J. Yang, L. P. Zhu, J. Chen, J. J. Shao, L. Liu, Z. L. Wang, *Mater. Today* **2018**, *21*, 88; f) X. Li, J. Tao, X. Wang, J. Zhu, C. Pan, Z. L. Wang, *Adv. Energy Mater.* **2018**, *8*, 1800705; g) L. Xu, T. Jiang, P. Lin, J. J. Shao, C. He, W. Zhong, X. Y. Chen, Z. L. Wang, *ACS Nano* **2018**, *12*, 1849; h) S. L. Zhang, M. Xu, C. Zhang, Y.-C. Wang, H. Zou, X. He, Z. Wang, Z. L. Wang, *Nano Energy* **2018**, *48*, 421.

[11] T. X. Xiao, X. Liang, T. Jiang, L. Xu, J. J. Shao, J. H. Nie, Y. Bai, W. Zhong, Z. L. Wang, *Adv. Funct. Mater.* **2018**, *28*, 1802634.

[12] a) T. Jiang, Y. Yao, L. Xu, L. Zhang, T. Xiao, Z. L. Wang, *Nano Energy* **2017**, *31*, 560; b) T. X. Xiao, T. Jiang, J. X. Zhu, X. Liang, L. Xu,

J. J. Shao, C. L. Zhang, J. Wang, Z. L. Wang, *ACS Appl. Mater. Interfaces* **2018**, *10*, 3616.

[13] a) T. Zhou, L. Zhang, F. Xue, W. Tang, C. Zhang, Z. L. Wang, *Nano Res.* **2016**, *9*, 1442; b) S. Wang, Y. Xie, S. Niu, L. Lin, C. Liu, Y. S. Zhou, Z. L. Wang, *Adv. Mater.* **2014**, *26*, 6720.

[14] a) A. Ahmed, Z. Saadatnia, I. Hassan, Y. Zi, Y. Xi, X. He, J. Zu, Z. L. Wang, *Adv. Energy Mater.* **2017**, *7*, 1601705; b) K. C. Neoh, G. D. Han, M. Kim, J. W. Kim, H. J. Choi, S. W. Park, J. H. Shim, *Nanotechnology* **2016**, *27*, 185403; c) S. H. Salter, *Nature* **1974**, *249*, 720.

[15] a) M.-L. Seol, J.-H. Woo, D.-I. Lee, H. Im, J. Hur, Y.-K. Choi, *Small* **2014**, *10*, 3887; b) H. Guo, J. Chen, L. Tian, Q. Leng, Y. Xi, C. Hu, *ACS Appl. Mater. Interfaces* **2014**, *6*, 17184.

1800514 (10 of 10)